

Reducing grid peak load through the coordinated control of battery energy storage systems located at electric vehicle charging parks

Daniel Kucevic^{a,*}, Stefan Englberger^a, Anurag Sharma^b, Anupam Trivedi^c, Benedikt Tepe^a, Birgit Schachler^d, Holger Hesse^a, Dipti Srinivasan^c, Andreas Jossen^a

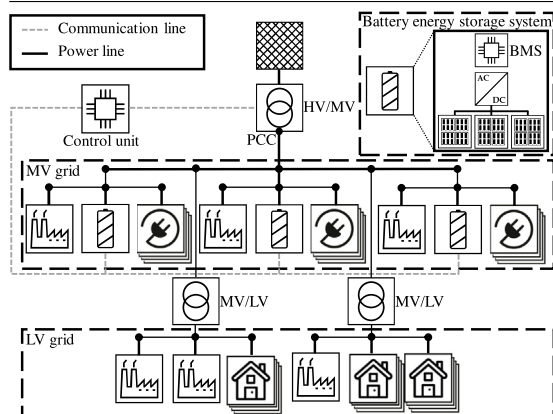
^a Institute for Electrical Energy Storage Technology, Technical University of Munich (TUM), Arcisstr. 21, 80333 Munich, Germany

^b Newcastle University in Singapore (NU), 172A Ang Mo Kio Avenue 8, 567739, Singapore

^c Department of Electrical and Computer Engineering, National University of Singapore (NUS), 4 Engineering Drive 3, 117583, Singapore

^d Reiner Lemoine Institute gGmbH (RLI), Rudower Chaussee 12, 12489 Berlin, Germany

GRAPHICAL ABSTRACT



ARTICLE INFO

Keywords:

Battery energy storage system
Lithium-ion
Grid integrated energy storage
Electric vehicle charging
Linear optimization
Distribution grid
Peak load reduction

ABSTRACT

Both global climate change and the decreasing cost of lithium-ion batteries are enablers of electric vehicles as an alternative form of transportation in the private sector. However, a high electric vehicle penetration in urban distribution grids leads to challenges, such as line over loading for the grid operator. In such a case installation of grid integrated storage systems represent an alternative to conventional grid reinforcement. This paper proposes a method of coordinated control for multiple battery energy storage systems located at electrical vehicle charging parks in a distribution grid using linear optimization in conjunction with time series modeling. The objective is to reduce the peak power at the point of common coupling in existing distribution grids with a high share of electric vehicles. An open source simulation tool has been developed that aims to couple a stand alone power flow model with a model of a stand alone battery energy storage system. This combination of previously disjointed tools enables more realistic simulation of the effects of storage systems in different operating modes on the distribution grid. Further information is derived from a detailed analysis of the storage system based on six key characteristics. The case study involves three charging parks with various sizes of coupled storage systems in a test grid in order to apply the developed method. By operating these storage systems using the coordinated control strategy, the maximum peak load can be reduced by 44.9%. The rise in peak load reduction increases linearly with small storage capacities, whereas saturation behavior can be observed above 800 kWh.

* Corresponding author.

E-mail address: daniel.kucevic@tum.de (D. Kucevic).

<https://doi.org/10.1016/j.apenergy.2021.116936>

Received 27 January 2021; Received in revised form 12 March 2021; Accepted 4 April 2021

Available online 30 April 2021

0306-2619/© 2021 The Authors. Published by Elsevier Ltd. This is an open access article under the CC BY license (<http://creativecommons.org/licenses/by/4.0/>).

Abbreviations

AC	Alternating current
BESS	Battery energy storage system
BMS	Battery management system
C	Carbon/graphite
DC	Direct current
eDisGo	Software for electric distribution grid optimization
EV	Electric vehicle
FEC	Full equivalent cycle
HV	High voltage
LFP	Lithium-iron-phosphate
LIB	Lithium-ion battery
lp_opt	Linear programming optimization tool for energy storage systems
LV	Low voltage
MV	Medium voltage
open_BEA	Open battery models for electrical grid applications
PCC	Point of common coupling
SimSES	Simulation of stationary energy storage systems
SOE	State of energy
V2G	Vehicle-to-grid

Sets & indices

B	Total number of nodes b in the distribution grid
b	Nodes in the distribution grid
b_j	Specific node b at location j in the distribution grid
b_k	Specific node b at location k in the distribution grid
H	Time vector for the simulation period (time horizon)
N	Vector for all nodes in the distribution grid
T	Time horizon
t	Specific time step

Parameters & variables

$\cos \varphi$	Power factor: ratio of real power to apparent power
η_b	Efficiency between the point of common coupling and a specific node b
η_{PE}	Efficiency of the power electronics
$E_t^{\text{actual},b}$	Actual energy content of a battery energy storage system at a specific node b for a specific time step t
$E_t^{\text{charge},b}$	Charged energy of a battery energy storage system at a specific node b for a specific time step t
$E_t^{\text{discharge},b}$	Discharged energy of a battery energy storage system at a specific node b for a specific time step t
E^{nominal}	Nominal energy content of a battery energy storage system
e^{rate}	Energy rate of the battery energy storage system
$\mathbf{I}^{b_j \rightarrow b_k}$	Vector for the line current between two specific nodes b (b_j and b_k) for each time step t before integrating charging parks

$\mathbf{I}_t^{b_j \rightarrow b_k}$	Line current between two specific nodes b (b_j and b_k) for a specific time step t before integrating charging parks
$\mathbf{I}^{*,b_j \rightarrow b_k}$	Vector for the line current between two specific nodes b (b_j and b_k) for each time step t after integrating charging parks
$I_{\text{max}}^{b_j \rightarrow b_k}$	Rated (maximum) line current between two specific nodes b (b_j and b_k)
$\mathbf{I}_t^{*,b_j \rightarrow b_k}$	Line current between two specific nodes b (b_j and b_k) for a specific time step t after integrating charging parks
$P_t^{\text{charge},b}$	Charging power of a battery energy storage system at a specific node b for a specific time step t
$P_t^{\text{discharge},b}$	Discharging power of a battery energy storage system at a specific node b for a specific time step t
P^{rated}	Rated power of the power electronics
S	Matrix for the apparent power at each node b for each time step t before integrating charging parks
$\mathbf{S}^{*,\text{PCC}}$	Vector of the apparent power at the point of common coupling for each time step t after integrating charging parks
$S_t^{*,\text{PCC}}$	Apparent power at the point of common coupling for a specific time step t after integrating charging parks
S_t^b	Apparent power at a specific node b for a specific time step t before integrating charging parks
\mathbf{S}^{CP}	Matrix for the charging park power at each node b for each time step t
$S_t^{\text{CP},b}$	Charging park power at a specific node b for a specific time step t
\mathbf{S}^{PCC}	Vector of the apparent power at the point of common coupling for each time step t before integrating charging parks
S_t^{PCC}	Apparent power at the point of common coupling for a specific time step t before integrating charging parks
SOE^{max}	State of energy upper limit
SOE^{min}	State of energy lower limit
U	Single phase voltage

1. Introduction

Renewable energy sources and EVs are seen as future key drivers of a substantial decrease in carbon emissions in both the transportation and power generation sectors [1]. However, this transformation poses new challenges to the power grid [2]. While in rural areas, the increased share of renewable energies, resulting in over voltages is the main cause of grid reinforcement [3], in urban distribution grids, it is forecast by the European Federation for Transport and Environment, that the number of public chargers in the EU will increase from 185000 public chargers to 1.3 million in 2025 and 2.9 million in 2030 [4].

Furthermore, an increased demand for DC fast charging units is predicted in the report for urban areas in particular [4]. This is motivated by the increasing prioritization of shared cars or electric taxis in these urban areas. They recommend introducing charging parks at easily accessible locations, with dedicated parking spots for electric taxis and shared EVs, notably in cities. Nicholas and Wappelhorst estimate

in a report about regional charging infrastructure requirements that the number of DC fast charging stations in Germany will quadruple from about 2000 in 2018 to about 8000 in 2030 [5]. Both studies as well as recently published papers [6,7] identified that existing grid infrastructure is not capable to include the additional power of such charging parks. While this paper examines the possibility of reducing peak power at the PCC in distribution grids in urban areas using coordinated controlled BESSs located at these charging parks, different other approaches are currently being discussed in the literature, both with and without BESS, that aim to meet these challenges.

First, conventional grid reinforcement or transformer upgrading may enable the integration of more EVs, as investigated by Brinkel et al. [8]. It was shown with a multi-objective optimization that in most cases, the advantages of EV charging with a higher transformer capacity limit do not outweigh the disadvantages, such as the costs and emissions generated by reinforcing the transformer. In their analysis, Pudjianto et al. [9] forecast in their study related to Great Britain's distribution grid that massive grid reinforcement will be required, costing up to £36bn by 2050. They propose a number of various smart charging strategies to reduce the costs, but none of these are able to eliminate grid reinforcement completely.

Second, several vehicle-to-grid (V2G) approaches exist by which to reduce the peak power in distribution grids. V2G enables bidirectional power flow at a charging station. An overview of the V2G concept and possible V2G services is presented by both Tan et al. [10] and Kempton et al. [11]. Sovacool et al. [12] have published a review of the neglected social dimensions, such as user behavior and acceptance. They conclude that neither the political framework nor the interest of consumers is taken into account in the majority of V2G approaches. Another disadvantage is the impact of V2G applications on vehicle battery lifetime due to a higher cyclic aging, as proposed by Wang et al. [13] and Jafari et al. [14].

Third, a number of researchers, such as Hanemann et al. [15,16] are examining the effect of using different smart charging strategies. The authors describe the impact on the power grid of applying a number of different EV charging strategies and conclude that as a side effect the curtailment of renewable energy sources can be reduced by smart charging strategies. However, they focus on the effects on spot market and CO₂ prices rather than on the effect on the distribution grid. The studies by Mehta et al. focuses on how to achieve optimal integration of EVs in a distribution grid [17,18]. Their strategies achieve both economic benefits in terms of daily costs and technical benefits in terms of peak load reduction and optimized active and reactive power flow. As with the V2G strategies, however, it must also be assumed here that users will provide their EVs for those smart charging strategies and therefore expect longer charging times.

Finally, BESS can also be used as an alternative to conventional grid reinforcement. The various approaches and their advantages and disadvantages will be discussed in more detail in the following. A general overview of state-of-the-art stationary BESSs based on lithium-ion batteries (LIBs) is provided among others by Diouf et al. [19] and Hesse et al. [20].

In the context of state-of-the-art peak shaving, Gimelli et al. [21] and Martins et al. [22] have investigated on an optimal sizing and design of the BESS, but neither has examined the effects on the distribution grid.

Reihani et al. [23] conducted an analysis of peak shaving on an island in Hawaii with a high share of renewable energy sources. Here, however, the focus was more on forecasting than on operation of the BESS itself. The work by Schram et al. [24] and Nykamp et al. [25] focuses on the behavior of a single BESS operated in a peak shaving application. Chapaloglou et al. [26] and Prvins et al. [27] both introduced a novel approach to an optimized energy management algorithm for peak shaving applications in selected distribution grids.

Summarizing the literature, there seems to be a consensus that a high EV-share is coming along with an increased number of charging

parks requires adaptations or new solutions in the power grid, especially in urban areas. None of the authors mentioned have considered the possibility of coupling multiple BESSs to reduce the peak power at the PCC in existing distribution grids and consequently to avoid or decelerate grid reinforcement requirements.

1.1. Scope of the study

This paper presents a method of reducing the peak power at the PCC in existing urban distribution grids in which a high share of EVs results in an increasing energy demand. A number of BESSs are located at various charging parks where the energy management systems are coordinated controlled with the aid of a linear optimization framework (lp_opt) which was adapted and expanded in the context of this study [28]. The stress on the stationary BESSs is evaluated by adapting a software framework for storage systems (SimSES) [29]. The impact on the distribution grid is analyzed by using a simulation tool for electric distribution grid optimization (eDisGo) [30].

This combination of previously disjointed tools within a newly developed interconnected simulation framework (open_BEAS) leads to a more realistic simulation of the effects of BESSs over different locations on the distribution grid. The coordinated control method developed in this study is applied to an exemplary grid that comprises a MV grid with 146 underlying LV grids [30]. The charging parks are located by the MV grid, and the results are compared with a state-of-the-art peak shaving strategy for each BESS, initially developed by Oudalov et al. [31]. The MV grid is connected to the high voltage (HV) level via a transformer at a single substation (PCC). Both the peak load of the charging parks and the nominal energy of the BESSs are varied to analyze the effects in different cases. Fig. 1 illustrates the scope of the paper in detail.

The highlights of this paper can be summarized as follows:

- A new framework called open_BEAS is developed to connect previously disjointed tools to enable accurate co-simulations of BESSs and distribution grids.
- The impact of BESSs, located at charging parks, is evaluated on the basis of peak load reduction at the PCC with varying EV-share and BESS capacities.
- A strategy is developed to control and coordinate the charging and discharging of the BESSs. The method is applied to a test distribution grid and compared with a state-of-the-art peak shaving strategy.
- Each BESS is evaluated using various key performance indicators along with its impact on the distribution grid.
- It is shown that the coordinated control strategy can significantly reduce the peak load on the PCC. This opens up new possibilities, allowing the grid operator to avoid grid reinforcement without influencing EV owners with reduced charging power or V2G strategies.
- The open-source code available to the research community is easily adaptable with individual parameter sets. Consequently, researchers or grid operators can use the method on their own storage systems or grid areas with individual charging park locations.

1.2. Outline of the paper

The remainder of this paper is structured as follows: Section 2 describes the open-source simulation tools eDisGo, SimSES and open_BEAS. The problem formulation, objective function and constraints are presented in Section 3. Section 4 gives an overview of the test distribution grid, the origin of the input profiles and the settings applied in this study. The results of the simulations are presented and discussed in Section 5, while Section 6 concludes the paper with an outlook of future work.

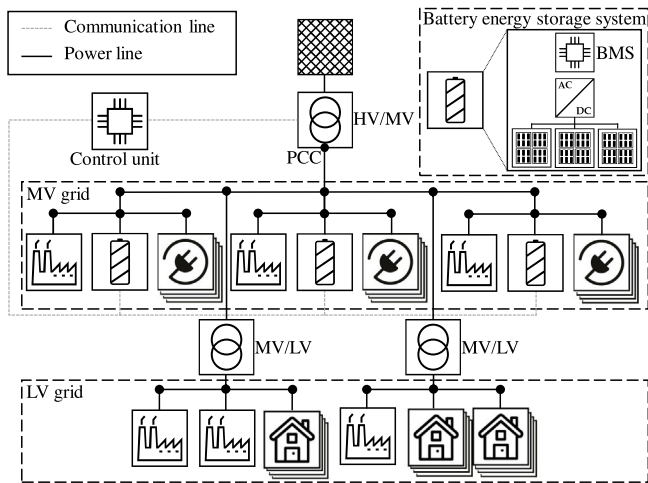


Fig. 1. Graphical overview of the paper. Several battery energy storage systems (BESSs), modeled in detail as shown in the blow-up, located at three different charging parks, are able to communicate with each other. They are coordinated and controlled by a central control unit to reduce the peak power at the point of common coupling (PCC).

2. Simulation framework and methodology

This section describes the newly developed interconnected simulation framework *open_BEAs*, the expanded linear programming optimization tool *lp_opt* and the adaptation of the existing tools (*eDisGo*, *SimSES*), which are used in this study. Fig. 2 is a schematic representation of the functionalities and the information flows of the four different tools. All simulation tools used in this study are entirely open-source.^{1,2} A description of further functionalities of all simulation tools can be found in Appendix A.

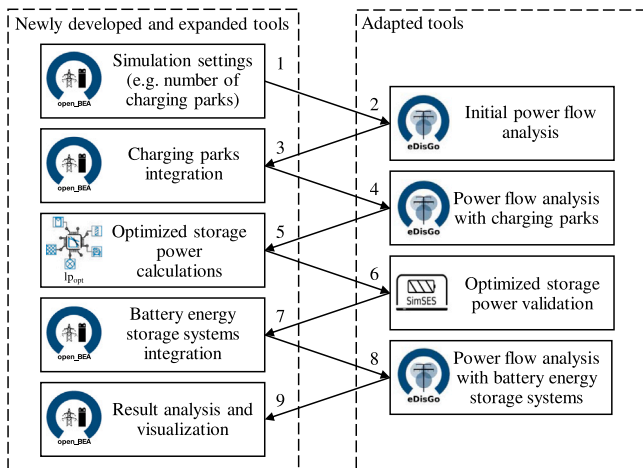


Fig. 2. Flowchart of all open-source simulation tools developed, expanded or adapted for use in this study. The newly developed tool *open_BEAs* operates as both a central control unit and a configuration unit. The adapted tools *eDisGo* and *SimSES* are validation tools for both the distribution grid and the battery energy storage systems (BESSs). With the help of *lp_opt* the energy management of all BESSs is controlled coordinated.

The purpose of the individual simulation tools and the flow of information and data is described step by step below:

¹ *open_BEAs*, *SimSES* and *lp_opt*: <https://www.ei.tum.de/en/ees/research-teams/team-ses/system-analytics-and-integration/>.

² *eDisGo*: <https://github.com/openego/eDisGo>.

- Initial setting:** Within the newly developed open-source simulation tool *open_BEAs*, the initial setting including the simulation duration, step size, and test grid is defined. Individual load demands are assigned to the various actors in the grid, such as domestic or industrial consumers.
- Initial power flow analysis:** Based on the load demands from the first step, the *eDisGo* software performs a power flow analysis for a selected period. In this step, the power flow analysis is conducted without charging parks and storage systems. The power flow results for all steps at all nodes and lines as well as the power at the PCC are transferred back to *open_BEAs* for the next simulation step.
- Charging parks integration:** In addition to the first step, the number, locations, and load time series of charging parks are defined and integrated into the simulated grid.
- Power flow analysis including charging parks:** Here, the *eDisGo* software performs a power flow analysis with charging parks. The power flow results for all steps at all nodes and lines as well as the power at the PCC are again transferred back to *open_BEAs* for the next simulation step.
- Optimized BESSs power calculations:** Within *open_BEAs*, the linear optimization tool *lp_opt* is launched. The expanded tool calculates an operation strategy for each BESS, limited by linearized constraints due to the distribution grid and the BESS. Aiming to reduce the peak power at the PCC, a linearized power flow from the BESSs to the PCC is assumed within the tool. The (dis-)charging strategy is introduced in Section 3.
- BESSs validation:** The tool *SimSES* is used for validating BESS time series from the optimized BESSs power calculations. This enables both the losses and the degradation to be determined and allows the data (time series) to be fed back to *open_BEAs*.
- BESSs integration:** In addition to step 3 BESSs including their dis(-)charging time series, located at charging parks, are integrated into the simulated grid.
- Power flow analysis including BESSs:** Here, the *eDisGo* software performs a power flow analysis with charging parks and BESSs. The power flow results for all steps at all nodes and lines as well as the power at the PCC are again transferred back to *open_BEAs* for the analysis and visualization. This step is necessary to validate the linearized power flow from step 5.
- Result analysis and visualization:** Finally, the effects of the charging parks and the BESSs on the power flow at the PCC are analyzed. In addition, the stress on the BESSs are evaluated using a defined set of key performance indicators.

3. Problem formulation and coordinated control strategy

3.1. Problem definition

An increased number of charging stations can cause higher load peaks in distribution grids, which can subsequently lead to overloading of existing grids. BESSs are a possible solution in order to avoid grid reinforcement and avoid influencing EV owners with reduced charging power or V2G strategies. While at present BESSs usually work in stand alone mode in accordance with state-of-the-art peak shaving, this study shows the possibility of reducing peak power at the PCC in distribution grids in urban areas using coordinated controlled BESSs located at charging parks. The following sections describe the strategy used to reduce the peak power of the HV/MV transformer (PCC).

Fig. 3 shows an extended graphical representation of the study along with an overview of all denotations of the optimization framework developed in this section. A variable marked with an asterisk (*) indicates that charging parks are included. Each charging park is equipped with a BESS. The BESSs are operated by a central control unit developed as part of this study, which can access the load at the PCC, the line loads and the demand of the charging parks. The central controller unit calculates a (dis-)charging strategy for each BESS, limited by a handful constraints due to the distribution grid and the BESS.

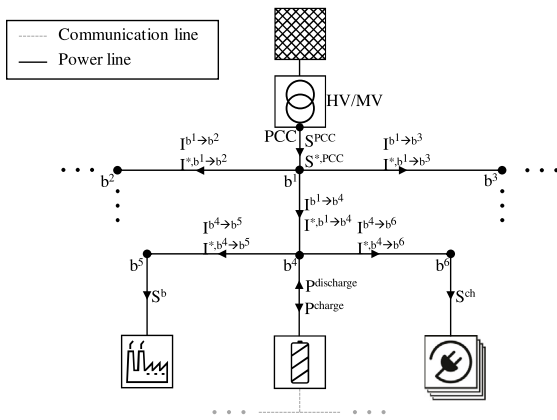


Fig. 3. Extended graphical representation of this study including all denotations from the optimization framework. A variable marked with an asterisk (*) indicates that charging parks are included.

3.2. Problem formulation

Eq. (1) defines the vector \mathbf{N} for all nodes b within the described distribution grid, with a total number of nodes B :

$$\mathbf{N} = [1, \dots, b, \dots, B]^T \quad (1)$$

The time step t within a defined time horizon T is defined by a vector \mathbf{H} as shown in Eq. (2):

$$\mathbf{H} = [1, \dots, t, \dots, T] \quad (2)$$

The apparent power S_t^b at each node b for each time step t before integrating charging parks is defined by a matrix \mathbf{S} (Eq. (3)):

$$\mathbf{S} = \begin{pmatrix} S_1^1 & \dots & S_t^1 & \dots & S_T^1 \\ \vdots & \ddots & \vdots & \ddots & \vdots \\ S_1^b & \dots & S_t^b & \dots & S_T^b \\ \vdots & \ddots & \vdots & \ddots & \vdots \\ S_1^B & \dots & S_t^B & \dots & S_T^B \end{pmatrix} \quad (3)$$

The current $I_t^{b_j \rightarrow b_k}$ for a specific line between two specific nodes b_k and b_j at each time step t before integrating charging parks is defined by a vector $\mathbf{I}^{b_j \rightarrow b_k}$ as shown in Eq. (4). If two nodes are not linked to each other, this value in the matrix remains 0:

$$\mathbf{I}^{b_j \rightarrow b_k} = [I_1^{b_j \rightarrow b_k}, \dots, I_t^{b_j \rightarrow b_k}, \dots, I_T^{b_j \rightarrow b_k}] \quad \forall b_j \in \mathbf{N}, b_k \in \mathbf{N}, b_j \neq b_k \quad (4)$$

The apparent load S_t^{PCC} at the PCC for each time step t before integrating charging parks is defined by a vector \mathbf{S}^{PCC} (Eq. (5)):

$$\mathbf{S}^{PCC} = [S_1^{PCC}, \dots, S_t^{PCC}, \dots, S_T^{PCC}] \quad (5)$$

The charging park power $S_t^{CP,b}$ for each time step t at each node b for each charging park with a coupled BESS results in a power matrix \mathbf{S}^{CP} as shown in Eq. (6). If a node has no charging park, this value in the matrix remains 0:

$$\mathbf{S}^{CP} = \begin{pmatrix} S_1^{CP,1} & \dots & S_t^{CP,1} & \dots & S_T^{CP,1} \\ \vdots & \ddots & \vdots & \ddots & \vdots \\ S_1^{CP,b} & \dots & S_t^{CP,b} & \dots & S_T^{CP,b} \\ \vdots & \ddots & \vdots & \ddots & \vdots \\ S_1^{CP,B} & \dots & S_t^{CP,B} & \dots & S_T^{CP,B} \end{pmatrix} \quad (6)$$

The apparent load $S_t^{*,PCC}$ at the HV/MV transformer (PCC) for the time horizon T after integrating charging parks at various nodes b is defined by a vector $\mathbf{S}^{*,PCC}$ in Eq. (7):

$$\mathbf{S}^{*,PCC} = [S_1^{*,PCC}, \dots, S_t^{*,PCC}, \dots, S_T^{*,PCC}] \quad (7)$$

The same applies to the matrix $\mathbf{I}^{*,b_j \rightarrow b_k}$, i.e. the current $I_t^{*,b_j \rightarrow b_k}$ for each line after integrating charging parks at various nodes b (Eq. (8)):

$$\mathbf{I}^{*,b_j \rightarrow b_k} = [I_1^{*,b_j \rightarrow b_k}, \dots, I_t^{*,b_j \rightarrow b_k}, \dots, I_T^{*,b_j \rightarrow b_k}] \quad \forall b_j \in \mathbf{N}, b_k \in \mathbf{N}, b_j \neq b_k \quad (8)$$

3.3. Coordinated control strategy

The objective is to minimize the peak apparent load $S_t^{*,PCC}$ at the PCC for the time horizon T after integrating charging parks at various locations b . Therefore the objective function is defined in Eq. (9):

$$\text{minimize : } \left\{ \max \left(S_t^{*,PCC} \right) \right\} \quad \forall t \quad (9)$$

The load at the PCC $S_t^{*,PCC}$ for all time steps t after integration of the charging parks with a coupled BESS is calculated in Eq. (10), while η_b is the efficiency between the PCC and a specific node b . The charging power $P_t^{\text{charge},b}$ and the discharging power $P_t^{\text{discharge},b}$ for a BESS at a specific node b are included in the coordinated control strategy together with a power factor $\cos \varphi$. The power factor $\cos \varphi$ and the efficiency η_b within the optimization framework (coordinated control strategy) is set to a constant factor (in this study to 1), which is necessary to perform a linear optimization:

$$S_t^{*,PCC} = S_t^{PCC} + \sum_{b \in \mathbf{N}} \left(\frac{S_t^{CP,b}}{\eta_b} + \frac{P_t^{\text{charge},b}}{\eta_b \cdot \cos \varphi} - \frac{P_t^{\text{discharge},b}}{\cos \varphi} \cdot \eta_b \right) \quad \forall t \quad (10)$$

The power of each BESS is only subject to the following restrictions in Section 3.5 and thus is controlled coordinated by this objective function aiming to minimize the peak power at the PCC.

3.4. Optimization constraints: Distribution grid

In addition to the objective function (Eq. (9)), the grid is subject to distribution line loading constraints. First of all, the line loads $I_t^{*,b_j \rightarrow b_k}$ have to be below their maximum rated current $I_{\max}^{b_j \rightarrow b_k}$ as shown in Eq. (11).

$$I_t^{*,b_j \rightarrow b_k} \leq I_{\max}^{b_j \rightarrow b_k} \quad \forall b_j \in \mathbf{N}, b_k \in \mathbf{N}, b_j \neq b_k \quad (11)$$

The line loads $I_t^{*,b_j \rightarrow b_k}$ after the charging park integration ($S_t^{CP,b}$) are calculated according to Eq. (12), where U is the single phase voltage.

$$I_t^{*,b_j \rightarrow b_k} = I_t^{b_j \rightarrow b_k} + \sum_{b \in \mathbf{N}} \left(\frac{S_t^{CP,b}}{U} + \frac{P_t^{\text{charge},b}}{U \cdot \cos \varphi} - \frac{P_t^{\text{discharge},b}}{U \cdot \cos \varphi} \right) \quad \forall t \quad (12)$$

3.5. Optimization constraints: Battery energy storage system

Furthermore, the BESS is also subject to a number of boundary conditions as described in the constraints Eqs. (13) – (17). The state of energy (SOE) must remain within the given bounds SOE^{\min} and SOE^{\max} . The nominal energy content of a BESS is denoted as E^{nominal} , and the actual energy content for a specific time step t of a BESS is denoted as $E_t^{\text{actual},b}$.

$$SOE^{\min} \cdot E^{\text{nominal}} \leq E_t^{\text{actual}} \leq SOE^{\max} \cdot E^{\text{nominal}} \quad (13)$$

The charging and discharging power ($P_t^{\text{charge},b}$ and $P_t^{\text{discharge},b}$) for each time step t and each BESS has to be lower than the respective maximum energy rate (e^{rate}) of the storage technology. In charging direction, the maximum e^{rate} is denoted as $E_t^{\text{charge},b}$ and in discharging direction as $E_t^{\text{discharge},b}$.

$$P_t^{\text{charge},b} \leq e_{\text{rate}}^{\text{charge}} \cdot E^{\text{nominal}} \quad \forall b \quad (14)$$

$$P_t^{\text{discharge}} \leq e_{\text{rate}}^{\text{discharge}} \cdot E^{\text{nominal}} \quad \forall b \quad (15)$$

The charging and discharging powers ($P_t^{\text{charge},b}$ and $P_t^{\text{discharge},b}$) are also limited by the rated power P^{rated} of the power electronics.

$$P_t^{\text{charge},b} \leq P^{\text{rated}} \quad \forall b \quad (16)$$

$$P_t^{\text{discharge},b} \leq P^{\text{rated}} \quad \forall b \quad (17)$$

The energy conservation of a BESS is defined in Eq. (18) and applies to any storage system at various nodes b . The actual energy content $E_t^{\text{actual},b}$ of a BESS depends on the energy content of the previous time step, the charged energy $E_t^{\text{charge},b}$ and the discharged energy $E_t^{\text{discharge},b}$.

$$E_t^{\text{actual},b} = E_{t-1}^{\text{actual},b} + E_t^{\text{charge},b} - E_t^{\text{discharge},b} \quad (18)$$

3.6. Reference case: State-of-the-art peak shaving

Motivated by a tariff system consisting of an energy and a power related component, the aim of state-of-the-art peak shaving is to minimize the maximum power peak value at one specific node b within a defined billing period. Particularly large electricity consumers with an annual demand above a certain limit (in Germany 100 MWh [32]) can reduce the peak power provided by the power grid, which directly results in reduced operating expenses in the form of reduced grid charges.

In order to reduce the peak power at a specific node b , the excess demand has to be covered by another power providing unit, such as a diesel generator or in our case a BESS. The BESS is used to decouple the supply and demand over a specified time. Consequently, it is essential to find a peak shaving threshold above which the power is provided by the BESS. First, a pre-processing linear optimization algorithm similar to that described in other publications [33,34] is used to minimize the power value of the peak shaving threshold $PS^{\text{threshold}}$, while complying with the necessary constraints, such as meeting the power demand and satisfying the energy and power specifications of the BESS. Secondly, the resulting peak shaving threshold is used as an input parameter for the operation strategy within the open_BEAS simulation tool.

In this study the state-of-the-art peak shaving strategy is used as follows: as long as the power of the consumer at a specific node b exceeds a specified threshold, the additionally required power is provided by the BESS. In addition, the BESS will recharge if the power value is below the previously determined optimal peak shaving threshold. This ensures that storage system charging does not cause the exceedance of the threshold. A more detailed description of the state-of-the-art peak shaving strategy is given by Martins et al. [22]. In Section 5, this state-of-the-art peak shaving strategy will be compared to the coordinated control strategy introduced in this study.

4. Test grid and applied settings

This section describes the test distribution grid and the applied settings used in the study. It also explains the main parameters of the example grid, the settings for the DC charging stations, and the load profiles used. Finally, it presents the settings and parameters relating to the BESS. However, the method presented in this paper is also applicable to other scenarios and grids.

4.1. Example grid

In order to apply and test the coordinated control strategy introduced in this paper, a synthetic test grid is selected consisting of a MV grid and 146 underlying LV grids [30]. This MV distribution grid is connected to the HV level via a transformer at a single substation (PCC), and the MV grid is operated as an open loop, which reflects the most common topology encountered in Germany [30]. The basic structure of the grid is presented in Table 1 and illustrated in Fig. 4.

Table 1

Parameters and settings of the synthetic distribution grid used in this study. The grid is connected to the high voltage level via a transformer at a single substation and is operated as an open loop.

Parameter/Setting	Number	Unit
Industrial consumers	82	–
Residential consumers	5787	–
Minimum annual consumption of a single consumer	1.3	MWh
Maximum annual consumption of a single consumer	7844.7	MWh
Total annual consumption excluding charging parks	31 953.0	MWh
Circuit breakers	4	–
LV lines	18 209	–
MV lines	225	–
Maximum load at the PCC	11.1	MW

4.2. Charging stations

The distribution of the charging stations is based on the work done by Luo et al. [35]. Accordingly, DC fast charging stations are mainly situated at locations with short parking times or those preferred by shared mobility users, such as shopping areas. We therefore allocated three charging parks in our test grid at different nodes that best fit these criteria. Fig. 4 shows the locations of the charging stations in the test grid.

A peak load of 350 kW is assumed for the DC fast charging units, which is in line with currently common fast chargers [36]. To evaluate different future scenarios, the DC fast charging stations at each of the charging parks were increased from two units to eight units. Accordingly, eight units are the equivalent of a peak load of 2.8 MW.

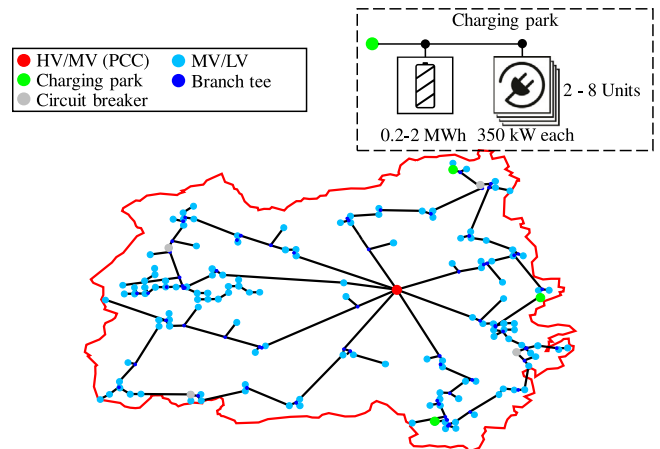


Fig. 4. Graphical representation of the test distribution grid showing the locations of the three charging parks with a battery energy storage system (BESS) connected (green). The circuit breakers are marked in gray, the MV/LV transformers are marked in light blue, the PCC in red and all branch tees in dark blue. As shown in the blow-up one BESS is connected to each charging park.

4.3. Load profiles

The simulation uses different load profiles for residential and industrial consumers. The 74 household loads used were created and published by HTW Berlin [37]. The industrial profiles are provided by industry partners of the Technical University of Munich. Of these, the three exemplary profiles that were determined as reference profiles in previous publications are used [38,39].

The load profiles of the EV charging stations have been examined by the Reiner Lemoine Institute. Based on the work of Nobis and Kuhnimhof [40], three different types of load profiles for charging parks have been defined. The profiles differ in time, frequency and peak load duration, depending on their position. Fig. 5 shows exemplary daily load profiles of the three charging parks used in this study.

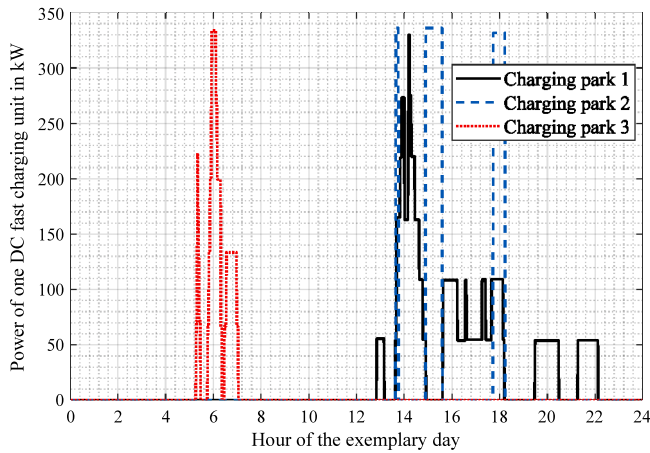


Fig. 5. Daily profile of the three different DC fast charging parks with an exemplary maximum power of 350 kW each.

The energy consumption of the charging parks is converted into a proportion of the total energy consumption (EV-share). For example, at each of the three charging park locations, the peak load is 700 kW, which corresponds to two DC fast charging units. This setting account for 4% (1.28 MWh) of the total energy consumption (31953 MWh as shown in Table 1) of the test distribution grid. With three DC fast charging units per charging location, the EV-share is 6%. The maximum EV-share considered in this study is 16%, which corresponds to eight DC fast charging units. Eight of these units are equivalent to a 2.8 MW peak load at each charging park, and this maximum was chosen so as not to exceed the maximum connection power to common MV nodes [41].

4.4. Battery energy storage system setting

The SimSES simulation tool, described in Appendix A.2 is used to validate the behavior of the BESS. The parameters and settings shown in Table 2 are used in this paper to represent and simulate a realistic BESS. A LIB with a lithium-iron-phosphate (LFP) cathode and a carbon/graphite (C) anode is selected [42]. This type of cell is particularly suitable for stationary applications due to its higher cycle durability [43,44]. The capacity of the BESS starts with 200 kWh increasing in increments of 200 kWh up to 2 MWh, again to ensure a connection to common MV nodes [41]

The power electronics (AC/DC converter) is modeled with a high efficiency above 10% of the rated power P_t^{rated} and the current charging power $P_t^{\text{charge,b}}$ or discharging power $P_t^{\text{discharge,b}}$ of a BESS, as shown in the example for charging case at a specific node b for a specific time step t in Eq. (19) [45]. In this study the following exemplary values are used: for the load dependent part $k = 0.0345$ and for the load independent part $p_0 = 0.0072$. The efficiency η_{PE} is independent of the direction of the power flow and there is no hysteresis. Maximum efficiency is attained at 0.46. P_t^{rated} with an efficiency of $\eta_{\text{PE}} = 96.9\%$. The maximum energy rate of the BESS (e^{rate}) in the discharging direction is set to a typical value of 2 h^{-1} . In accordance with the type of battery cell, the maximum e^{rate} in the charging direction is set to 1 h^{-1} . The battery management system (BMS) is configured such that the SOE remains within the range of 5-95%. The SOE at the beginning of the simulation is set to 50%.

$$\eta_{\text{PE}} = \frac{P_t^{\text{charge,b}}}{P_t^{\text{rated}} + p_0 + k \cdot \left(\frac{P_t^{\text{charge,b}}}{P_t^{\text{rated}}} \right)^2} \quad (19)$$

Table 2

Parameters and settings of the simulated battery energy storage system (BESS) comprising battery cells, a power electronics unit and a battery management system (BMS).

Parameter/Setting	Description/Value	Unit
Battery cell manufacturer	muRata	-
Battery cell type	US26650FTC1	-
Battery cell chemistry	LFP:C	-
Battery cell capacity	2850	mAh
Nominal cell voltage	3.2	V
Power electronics	cf. Eq. (19)	-
Maximum efficiency of power electronics	96.9	%
Maximum e^{rate} (discharge)	2	h^{-1}
Maximum e^{rate} (charge)	1	h^{-1}
Capacity per storage system	200-2000	kWh
SOE range	5-95	%
SOE start	50	%

4.5. Simulation settings

In order to take into account seasonal fluctuations, a simulation duration of six months from January to June is selected for the simulation. This enables reliable results (e.g. aging behavior) to be obtained for the BESS. The simulation step size chosen is 15 min. Hence, the profiles from Section 4.3, which have a higher time resolution, are averaged. The 15 min time steps represent a compromise between the duration of the simulation and the accuracy of the input profiles.

5. Results and discussion

This section discusses the impact of coordinated controlling the BESSs on the test distribution grid for a six months simulation period. For this purpose, the load flows and potential reductions in peak load at the PCC are evaluated in detail and compared to the results obtained with a state-of-the-art peak shaving algorithm. The effects of this and the resulting stress on the BESS are also investigated.

5.1. Reference case: State-of-the-art peak shaving

Fig. 6 shows the peak load change at the PCC in the form of a contour plot of a state-of-the-art peak shaving strategy, outlined in Section 3.6. Peak load reduction or increase in Fig. 6 refers to the scenario without charging parks (0% EV-share). The capacity of the BESS starts with 200 kWh increasing in increments of 200 kWh up to 2 MWh, while the EV-share increased in two percentage point steps from 4% to 16%. Positive values in the contour plot (dark blue areas) indicate the settings with a peak load reduction at the PCC, but since the BESSs are directly coupled to the charging parks and only shave the additional peaks occurring due to EVs, there are no significant peak reductions at the PCC.

Even if the BESSs are able to shave the entire peak, there are increases in the load at the PCC compared to the scenario without EVs, especially in an area with a high EV-share and large BESSs. These slight increases, indicated in yellow and red in Fig. 6, are due to the immediate recharging of the BESSs. This occurs especially when a charging park has already fallen below its peak shaving limit and the BESS is recharging, while the load at the PCC is still close to peak level. The additional power that the BESS at this point of time needs to recharge leads to an increase in the load at the PCC up to 7.5% compared to a scenario without EVs.

Hence, state-of-the-art peak shaving BESSs located at charging parks can help to avoid significant increases in the peak load at the PCC when the EV-share is rising, but it is these results, obtained for state-of-the-art peak shaving, which motivate the introduction of a coordinated and controlled strategy for the three BESSs.

Fig. 7 supports this statement, showing the power flow including the charging park load profiles at the PCC for one exemplary day for the

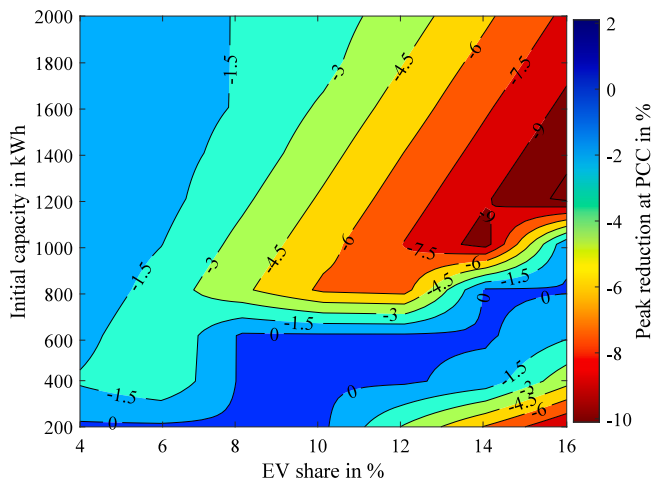


Fig. 6. Peak load reduction contour plot relating to a scenario without electric vehicles (EVs) at the point of common coupling (PCC) with increasing EV-share and battery energy storage systems (BESSs) of different sizes coupled to charging parks. The BESSs operate in stand alone mode in accordance with state-of-the-art peak shaving.

following scenario: 16% EV-share, and storage capacities of 800 kWh. The filled area ($Load_{PCC,PS}$) shows the power flow after including the charging parks and the BESSs are operating with a state-of-the-art peak shaving strategy. The charging parks are displayed in total ($Load_{CP,tot}$) and the load at the PCC is displayed both with ($Load_{PCC,withCP}$) and without ($Load_{PCC,woCP}$) charging parks. The first peak of the charging station between 5:00 and 8:00 am is contrary to the peak at the PCC without EVs ($Load_{PCC,woCP}$). Although this peak is shaved by the BESS unit using state-of-the-art peak shaving, there is no peak load reduction at the PCC, because the peak only occurs later that day. However, the peaks in the charging parks between 12 noon and 19:00 cause peaks in the distribution grid are not entirely shaved by the BESSs. By comparison with Fig. 5, it can be identified that only two out of three charging parks account for the additional peak, consequently only two BESSs are discharging in this time period and thus not the full available power of all three BESSs is used to reduce the peak load at the PCC.

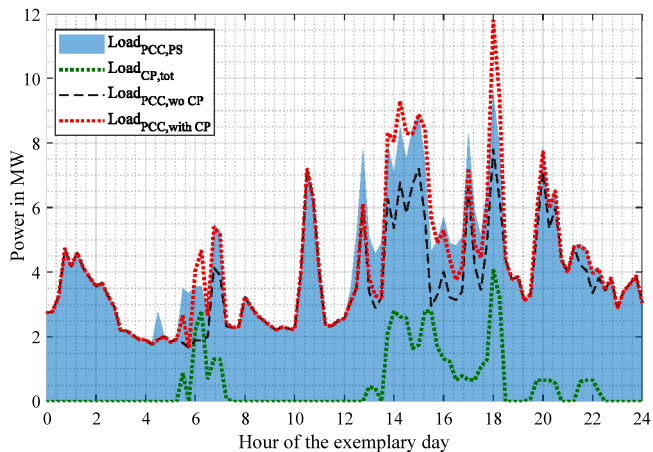


Fig. 7. Power flow including the charging park load profiles ($Load_{CP,tot}$) at the point of common coupling (PCC) for one exemplary day. The load at the PCC is displayed both with ($Load_{PCC,withCP}$) and without ($Load_{PCC,woCP}$) charging parks. The battery energy storage systems (BESSs) operate in stand alone mode in accordance with state-of-the-art peak shaving and the resulting power flow is showed as a filled area ($Load_{PCC,ps}$).

5.2. Coordinated control strategy: Distribution grid results

The settings and case studies described in Section 4 are tested under application of the presented coordinated control strategy. Fig. 8

illustrates the peak load change at the PCC as a contour plot. Peak load reduction or increase in Fig. 8 refers to the scenario without charging parks (0% EV-share). The capacity of each BESS starts with 200 kWh increasing in increments of 200 kWh up to 2 MWh, while the EV-share increased in two percentage point steps from 4% to 16%. Positive values in the contour plot (dark blue areas) indicate the settings with a peak load reduction at the PCC.

A trend can be seen, in that the greater the storage capacity, the greater the peak reduction. As mentioned in Section 4, the peak load in the test distribution grid without EVs is 11.1 MW and the maximum peak load reduction of 44.9% (dark blue area in Fig. 8) at the PCC compared to a scenario without EVs occurs at the largest BESS capacity (2 MWh each) and the smallest EV-share (4%). Although each BESSs could theoretically discharge up to 4 MW (cf. Table 2), which would be 12 MW in total, no higher peak load reduction can be achieved. The reason for this behavior is that the power capability of the BESS is usually the limiting factor for the high peaks, while the peaks in the test distribution grid are wider with a low shaving limit and thus the energy content is limited.

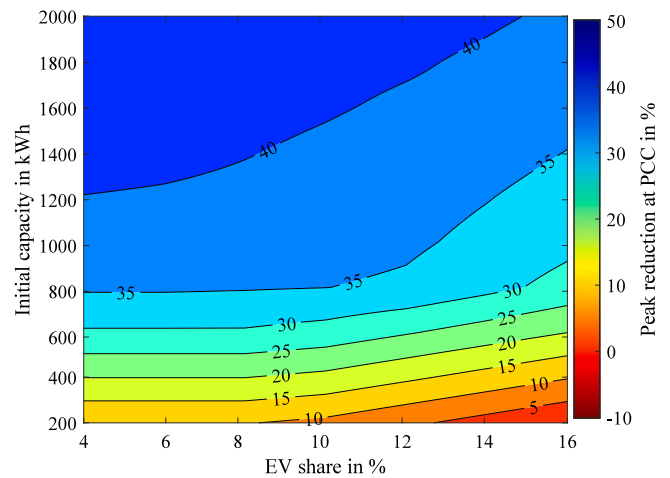


Fig. 8. Peak load reduction contour plot relating to a scenario without electric vehicles (EVs) at the point of common coupling (PCC) with an increasing EV-share and battery energy storage systems (BESSs) coupled to charging parks. The BESSs operate in accordance with the coordinated and coupled energy management system developed in this study.

However, the peak reduction only increases linearly up to a BESS capacity of 800 kWh, while saturation behavior sets in above 800 kWh BESS capacity. The trend lines for a given EV-share are shown in Fig. 9. Here, the abscissa shows the increasing BESS capacity, while the ordinate shows the peak load reduction relating to a scenario without EVs at the PCC. The reason for the saturation behavior is again that with higher BESS capacities and thus lower peak shaving limits the energy content is the limiting factor. With the physical link between energy and power not only the height of the power peak, but also the integral of the power needs to be covered by the BESSs. Up to an EV-share of 10%, charging parks are not responsible for peaks in the test distribution grid and for this reason, no differences can be seen in the trend lines in Fig. 9 for an EV-share of 4 to 8% up to a BESS capacity of 800 kWh.

This is supported by Table 3, where the peak load at the PCC is shown for all scenarios. However, from a storage size of 1 MWh onward, peaks that already include a power demand from the charging park can be shaved, resulting in slight differences in the trend lines. Only from 10% EV-share, the peak load at the PCC exceed the 11.1 MW of the initial scenario without EVs. In the test setting, the charging parks provide the highest peaks with 12.1 MW in the distribution grid with an EV-share of 16% as shown in Table 3. Nevertheless, even with a 16% EV-share, the three smallest simulated BESSs (200 kWh each) are able to ensure that the PCC is not subjected to greater peak loads than in a scenario without EVs.

Table 3

Peak load at the point of common coupling (PCC) in MW in the test distribution grid for a scenario without charging parks and for all case studies with and without battery energy storage systems (BESSs). The maximum load at the PCC is 11.1 MW without both charging parks and BESSs.

Initial capacity in kWh	EV-share in %		4		6		8		10		12		14		16	
			No	With												
	BESS	BESSs	BESS	BESSs	BESS	BESSs	BESS	BESSs	BESS	BESSs	BESS	BESSs	BESS	BESSs	BESS	BESSs
200		10.0		10.0		10.0		10.0		10.2		10.5		10.8		11.1
400		8.9		8.9		8.9		8.9		9.0		9.4		9.9		10.0
600		7.9		7.9		7.9		7.9		8.0		8.3		8.6		8.9
800		7.2		7.2		7.2		7.2		7.2		7.3		7.6		8.0
1000		6.9		6.9		6.9		7.0		7.0		7.1		7.4		7.7
1200	11.1	6.7	11.1	6.7	11.1	6.8		6.8	11.2	6.9	11.5	7.0	11.8	7.2	12.1	7.5
1400		6.5		6.6		6.7		6.7		6.8		6.9		7.0		7.3
1600		6.4		6.5		6.6		6.6		6.6		6.7		6.8		7.1
1800		6.3		6.4		6.4		6.4		6.6		6.6		6.8		6.9
2000		6.1		6.2		6.3		6.3		6.4		6.5		6.6		6.8

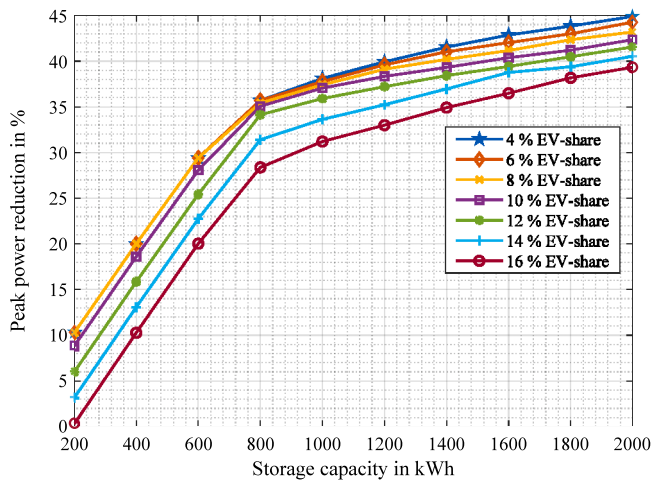


Fig. 9. Trend lines showing the reduction in peak load relating to a scenario without electric vehicles (EVs) at the point of common coupling (PCC) with an increasing EV-share and battery energy storage systems (BESSs) coupled to charging parks. The BESSs operate in accordance with the coordinated and coupled energy management system developed in this study.

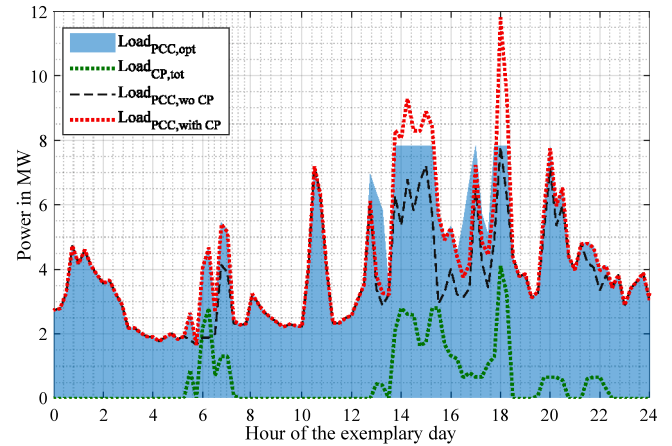


Fig. 10. Power flow including the charging park load profiles ($Load_{CP,tot}$) at the point of common coupling (PCC) for one exemplary day, is displayed both with ($Load_{PCC,withCP}$) and without ($Load_{PCC,woCP}$) charging parks. The battery energy storage systems (BESSs) operate in accordance with the coordinated and coupled strategy developed in this study and the resulting power flow is showed as a filled area ($Load_{PCC,opt}$).

Fig. 10 shows the power flow including the charging park load profiles at the PCC for one exemplary day for the following scenario: 16% EV-share, and storage capacities of 800 kWh. The filled area ($Load_{PCC,opt}$) shows the power flow after including the charging parks and the BESSs are operating with coordinated control strategy. The charging parks are displayed in total ($Load_{CP,tot}$) and the load at the PCC is displayed both with ($Load_{PCC,withCP}$) and without ($Load_{PCC,woCP}$) charging parks. The first peak of the charging station between 5:00 and 8:00 am is contrary to the peak at the transformer without EVs ($Load_{PCC,woCP}$). While this peak is shaved by the BESS unit using state-of-the-art peak shaving (cf. Fig. 7), the BESSs do not discharge with the coordinated and coupled strategy, since there would be no load reduction on the PCC.

The peaks in the charging parks between 12 noon and 19:00 cause peaks in the distribution grid which are shaved by the BESSs. The peak load at the PCC here is 7.9 MW, which corresponds to the 28.4% peak reduction in the scenario without EVs, as shown in the contour plot Fig. 8. Although each BESSs in this scenario could theoretically discharge up to 1.6 MW (cf. Table 2), which would be a load reduction of 4.8 MW in total (43.2%), no higher peak load reduction can be achieved. Due to the base load, the BESSs can no longer be fully recharged below a certain peak load limit. As can be seen from Fig. 10, with a lower peak load limit, the energy (area between peak load limit ($\max(Load_{PCC,opt})$) and $Load_{PCC,withCP}$) to be capped would increase and thus the energy content of the BESSs is limited.

5.3. Validation

All numbers in this study refer to results conducted with the non-linear power flow calculation tool eDisGo. However, as shown in Section 3.3, within the coordinated control strategy the power flow was linearized with the aim of performing a linear optimization. Fig. 11 shows the differences between the load flows calculated in the linear optimizer lp_{opt} and the load flows on the PCC validated with eDisGo. The differences are due to cable losses as well as to the non-linearity on the consumer side and the non-linearity at the power transmission. The maximum difference, however, is 0.23 MW, which corresponds to only 2.9% in relation to the maximum load on the PCC in the scenario without EVs.

When discussing about beneficial effects through coordinated BESS control, one should also consider the stress of a BESS. Fig. 12 shows the peak load reduction at the PCC per full equivalent cycle (FEC) for the six months simulation period. The FECs of all three BESSs are totaled. Two trends can be identified. First, the lower the BESS capacity, the greater the peak load reduction per FEC, and second, the lower the EV-share, the greater the peak load reduction per FEC. Consequently, small storage system with the only aim, reducing the peak power at the PCC are more efficient.

Analyzing the aforementioned trends in detail using a key characteristic of BESSs, it can be observed that BESSs with a capacity of less than 800 kWh are only subjected to a few FECs in the simulation period as shown in Fig. 13. This figure shows the mean number of FECs of

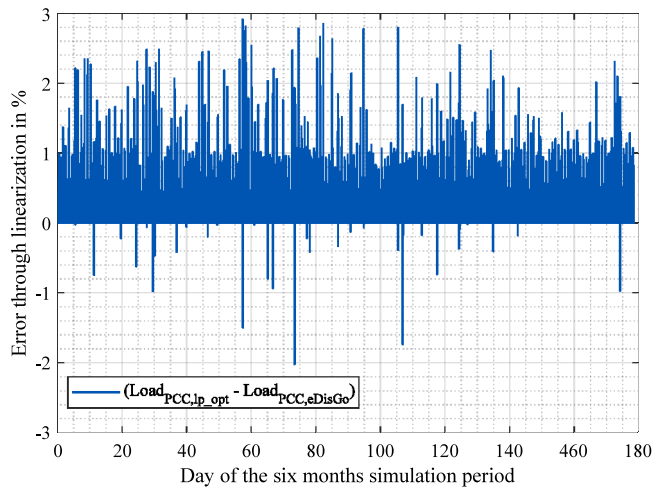


Fig. 11. Power flow comparison at the point of common coupling (PCC) between the power flow calculation used for the coordinate control strategy ($Load_{PCC,lp_opt}$) and the non-linear power flow calculation with eDisGo ($Load_{PCC,eDisGo}$) for the six month simulation period.

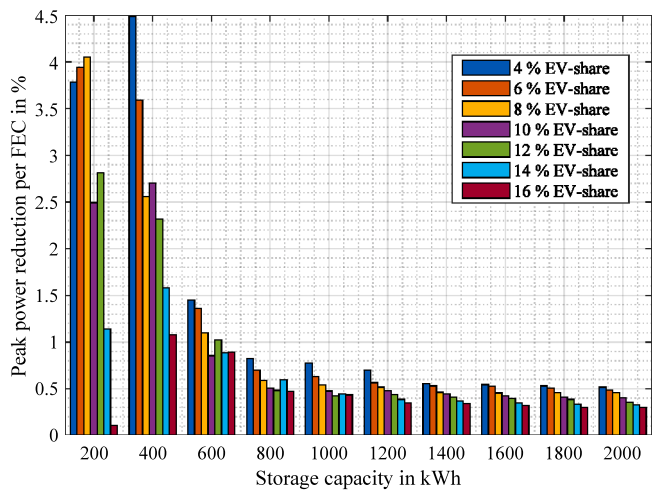


Fig. 12. Reduction in peak load relating to a scenario without electric vehicles (EVs) at the point of common coupling (PCC) per full equivalent cycle with increasing EV-share and battery energy storage systems (BESSs) coupled to charging parks. The BESSs operate in accordance with the coordinated and coupled energy management system developed in this study.

the three BESSs after a six month simulation period. Hence, due to the low stress, the BESSs remain most of the time in a high SOE range above 90%, which leads to an accelerated calendar degradation with the modeled battery cell [43].

However, as a result of the low stress, BESSs with an initial capacity below 800 kWh remain underutilized and it should be considered to use these for stacking multiple applications [46] - a topic beyond the scope of this study. Further analyses of storage behavior in different settings is presented in Appendix B, along with the six key characteristics from a previous publication [38].

6. Conclusion and outlook

This paper presents a method to reduce the power at the transformer or PCC in distribution grids with a high share of EVs. Charging parks are

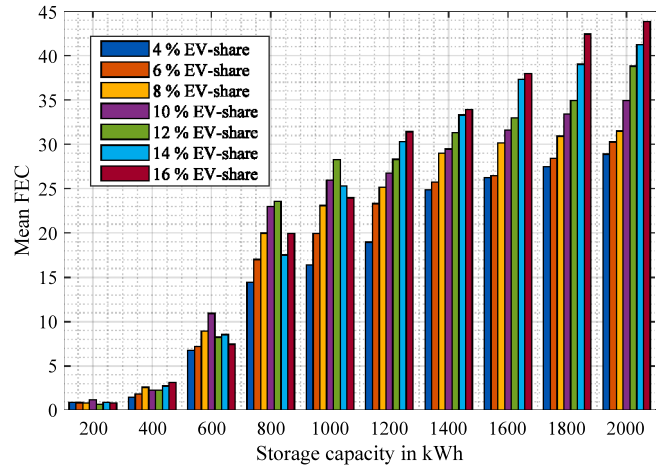


Fig. 13. Mean number of full equivalent cycles (FECs) of the three battery energy storage systems (BESSs) after a six month simulation period. The BESSs operate in accordance with the coordinated and coupled energy management system developed in this study.

located at three different nodes in a representative MV grid, and the EV-share varied in the course of a sensitivity analysis. At all three nodes, a BESS with various capacities is coupled and the attendant energy management system is controlled with the aid of a linear optimization framework, which was expanded as part of this study. The stress on the LIB based stationary BESSs is evaluated by adapting the holistic energy storage simulation framework SimSES, while the impact on the distribution grid is analyzed using the simulation tool eDisGo. The open_BEAs framework developed as part of this study connects these previously disjointed tools to enable accurate co-simulations of BESSs and distribution grids.

The objective function, which has been developed to control and coordinate the charging and discharging of the BESSs is applied to a test distribution grid comprising 1 MV grid and 146 underlying LV grids. In total, there are 82 industrial consumers and 5787 residential consumers. The EV-share in this study starts with 4%, which corresponds to two DC fast charging units at each charging park, and ends with 16%.

The capacity of the coupled BESSs increases from an initial level of 200 kWh to 2000 kWh. The BESS is simulated in detail with a LFP:C cell model that comprises a degradation model, a power electronics model with a representative efficiency curve and a BMS that is responsible for monitoring the maximum cell currents and SOE limits.

There are no peak reductions at the PCC if the BESSs are operated in a stand alone mode with a state-of-the-art peak shaving algorithm. There are even slight increases up to 7.5% of the load at the PCC compared to a scenario without EVs. For most scenarios, however, no or only a very small increase in the peak load can be identified. Hence, state-of-the-art peak shaving BESSs located at charging parks can help to avoid significant increases in the peak load at the PCC when the EV-share is rising. Furthermore, individual overloaded or limiting lines can be relieved with this operation mode.

If the BESSs is operated using the coordinated control method developed in this study, the peak load at the PCC can be reduced in all scenarios by a maximum of 44.9%. While the rise in peak reduction increases linearly with small BESS capacities, a saturation behavior can be observed above 800 kWh.

The power flow was verified with the eDisGo simulation tool, showing that for the test grid, the linearization in lp_opt produces similar results as the validated model. The maximum difference of 0.184 MW corresponds to 1.7% in relation to the maximum load on the PCC in the scenario without EVs.

Analyzing the results of the simulation tool for the BESS (SimSES) shows a clear trend, in that the peak load reduction per FEC decreases with an EV-share and BESS capacity increase. For a storage capacity of 200 kWh and a 4% EV-share, a reduction of 3.5% at the PCC can be achieved, compared to the scenario without EVs. For the largest BESS of 2000 kWh and the highest EV-share of 16%, the reduction is only 0.3% per FEC. Further key indicators such as the total number of FECs show, that BESSs with a capacity of less than 800 kWh are only subjected to a low stress and remain underutilized within the simulation period.

The method presented in this study was applied to an exemplary grid. The numerical results therefore only apply to this test area. However, the open-source simulation tools allow operators to investigate their own distribution grids, and test the impact of various BESS capacities and locations. Both the effect of state-of-the-art peak shaving and coupled storage systems can be analyzed with the framework developed in this study.

6.1. Future work and outlook

This study focuses on the technical potential of coupled energy management systems for a number of BESSs in a distribution grid. The reduction in the peak load at the PCC can avoid the need to exchange a transformer or reinforce cables. Future work can therefore focus on an economic analysis. For example, the cost of installing a BESS can be compared with the costs of conventional grid reinforcement.

In addition to an economic analysis, it might also be worthwhile to perform an ecological assessment to enable more precise investigation of the differences between conventional grid reinforcement and BESSs installation. While some studies, such as the work done by Baumann et al. [47], already deal with the CO₂ impact of BESSs, there is a research gap concerning the impact of CO₂ caused by conventional grid reinforcement.

Smart charging strategies or the potential of V2G at residential charging locations can be used to reduce the stress on the distribution grid resulting from a high EV-share. Therefore, the simulation tools presented in this study can be used to investigate the effect of these strategies on the distribution grid.

Existing peak shaving BESSs can lead to a peak load reduction at the PCC if the grid operator exchanges his current grid status with the BESS operator. However, this will require the creation of an economic and legal framework.

CRedit authorship contribution statement

Daniel Kucevic: Conceptualization, Methodology, Software, Writing - original draft, Visualization. **Stefan Englberger:** Methodology, Software. **Anurag Sharma:** Methodology, Writing - review & editing. **Anupam Trivedi:** Methodology, Writing - review & editing. **Benedikt Tepe:** Data curation. **Birgit Schachler:** Software. **Holger Hesse:** Supervision, Conceptualization, Writing - review & editing. **Dipti Srinivasan:** Supervision, Writing - review & editing. **Andreas Jossen:** Supervision, Writing - review & editing.

Declaration of competing interest

The authors declare that they have no known competing financial interests or personal relationships that could have appeared to influence the work reported in this paper.

Acknowledgments

This publication was financially supported by the German Federal Ministry for Economic Affairs and Energy within the research project open_BEA (Grant No. 03ET4072), which is managed by Project Management Jülich. The responsibility for this study rests with the authors.

Appendix A. Simulation framework: Additional description of further functionalities

A.1. Open battery models for electrical grid applications

The holistic open-source simulation tool open_BEA developed in this study enables BESS to be integrated into MV grids as well as LV grids in order to analyze the effects of the various operating strategies. The source code is programmed in Python. The main characteristic is the ability to assign individual time series to the various actors in the grid, such as domestic or industrial consumers. Furthermore, EV charging parks are integrated at various nodes to investigate the effects of increasing the share of electric mobility. open_BEA connects the following previous disjoint tools to enable accurate co-simulations of BESSs and distribution grids.

A.2. Simulation of stationary energy storage systems

SimSES, initially developed in MATLAB[®] [29], was converted to Python in 2019 and underwent enhancement at the EES institute at the Technical University Munich. SimSES enables the detailed simulation and evaluation of stationary energy storage systems, with the main focus currently on LIBs. The tool has been used in several publications, mainly for stand alone [48,49] or coupled [28] home energy storage systems, but also for peak shaving storage systems [22] or frequency containment reserve applications [38].

The main characteristic of this modular and flexible software tool is its abstract approach to the energy storage model, which enables the variation and hybridization of storage technologies and technical sub-components. In addition, stress characterization estimates the energy storage degradation. Various semi empirical aging models can be used for this purpose.

A.3. Software for electric distribution grid optimization

The purpose of the eDisGo software is to perform a power flow analysis for a certain time period. The processing of the input parameters (e.g. loads or line impedances) is done with eDisGo, while the single step non-linear power flow calculation is conducted using the open-source PyPSA software [50]. The eDisGo tool is implemented in Python and has been previously used in two studies [30,51].

Apart from this study, eDisGo enables to assess the potential of flexibility options as an economic alternative to conventional grid expansion. And thus to assess their potential in lower grid expansion needs that arise from an increase in both renewable capacities and new consumers in medium and low voltage grids. Hence, it is necessary in eDisGo to identify both the grid problems and the costs incurred.

A.4. Linear programming optimization tool for energy storage systems

Like SimSES, the lp_opt tool was developed at the Institute for Electrical Energy Storage Technology at the Technical University of Munich. With its flexible structure, it serves as a co-optimization framework for both stationary and mobile energy storage systems and their underlying operation strategies. The tool was designed in the MATLAB[®] optimization environment using a problem-based approach. Besides the mathematical optimization solver of MATLAB[®], the tool is also compatible with the Gurobi solver [52]. Both have been presented in previous literature [28,33].

The operation strategy of either an individual BESS or a multi-storage system with multiple BESSs can be optimized using lp_opt. Depending on the defined technical components of the observed energy

system, there are several entities that can be optimized and simulated, taking into consideration generating units, demand curves, EVs, their charging stations, and stationary BESSs.

Appendix B. Coordinated control strategy: Additional battery energy storage system results

Six characteristics defined in a previous publication are used to analyze the storage behavior in different settings [38]. The following figures all show the mean value (characteristic) of the three BESSs after a six months simulation period based on the setting defined in Section 4.

Fig. B.14 shows the remaining capacity in %, which is linked to the mean SOE (Fig. B.15) and the number of FEC (Fig. 13). The mean round-trip efficiency is displayed in Fig. B.16. The remaining characteristics describe the stress on the BESSs.

Fig. B.17 shows the average cycle depth in discharge direction. The number of alternations between charging and discharging (sign changes) per day is indicated in Fig. B.18, while Fig. B.19 shows the energy that is charged or discharged between sign changes, respectively. Finally, Fig. B.20 shows the average resting times.

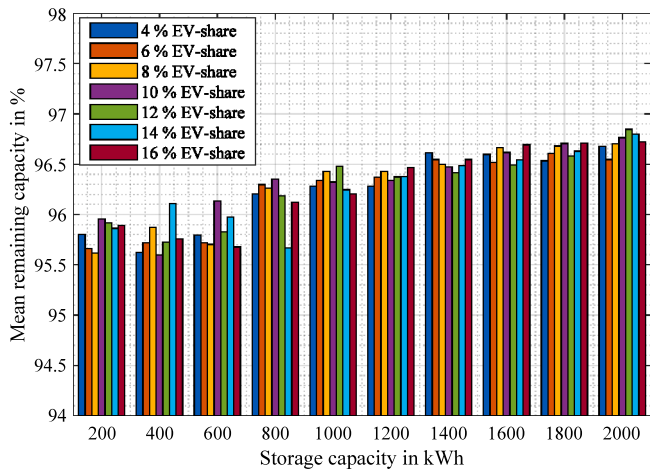


Fig. B.14. Mean remaining capacity of the three battery energy storage systems (BESSs) after a six month simulation period. The BESSs operate in accordance with the coordinated and coupled energy management system developed in this study.

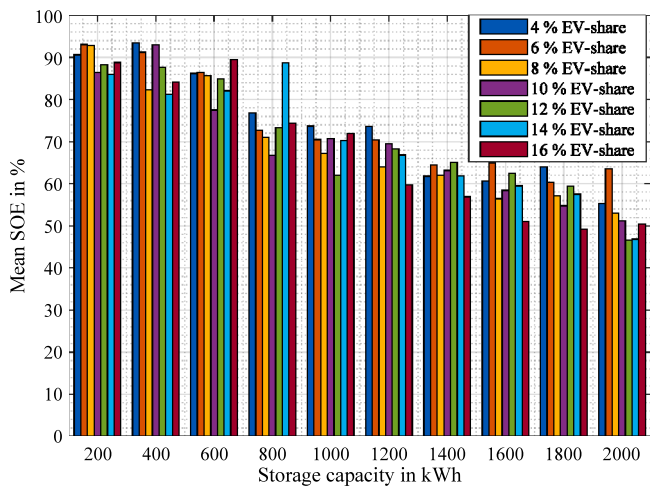


Fig. B.15. Mean state of energy of the three battery energy storage systems (BESSs) after a six month simulation period. The BESSs operate in accordance with the coordinated and coupled energy management system developed in this study.

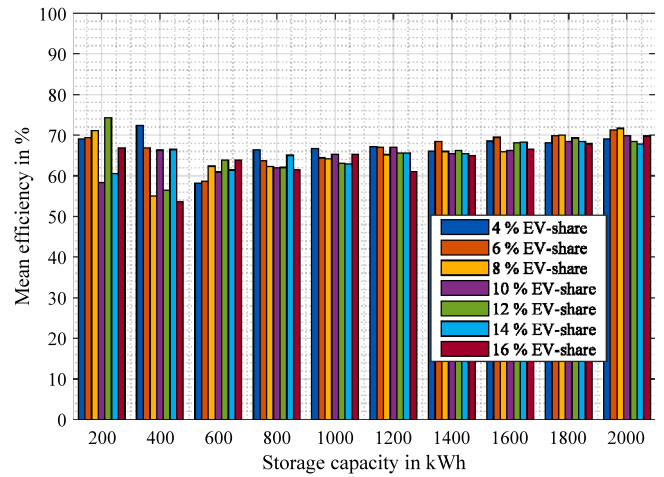


Fig. B.16. Mean efficiency of the three battery energy storage systems (BESSs) after a six month simulation period. The BESSs operate in accordance with the coordinated and coupled energy management system developed in this study.

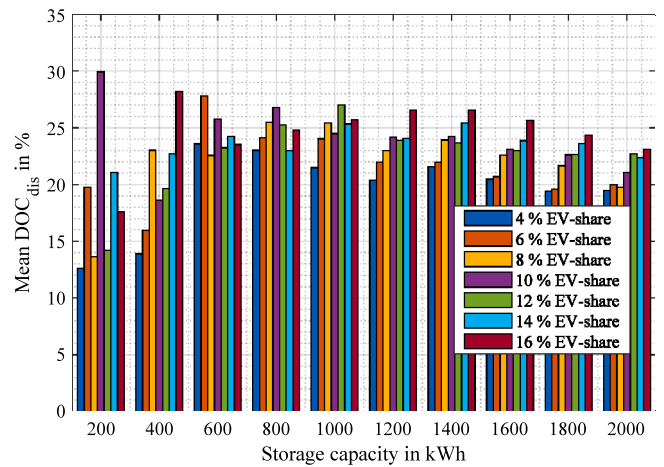


Fig. B.17. Mean depth of cycle in discharge direction of the three battery energy storage systems (BESSs) after a six month simulation period. The BESSs operate in accordance with the coordinated and coupled energy management system developed in this study.

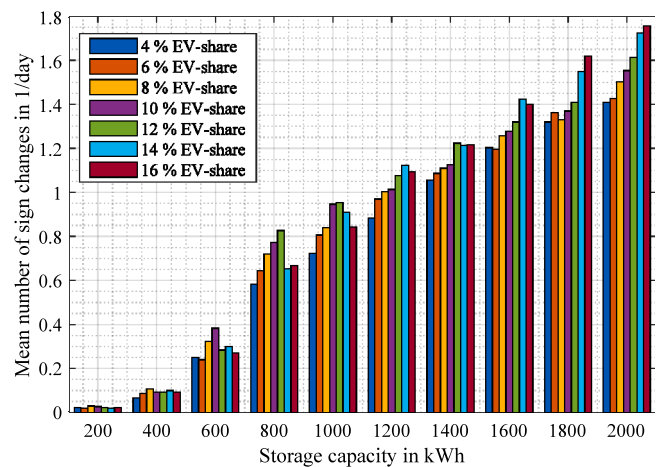


Fig. B.18. Average number of sign changes per day of the three battery energy storage systems (BESSs) after a six month simulation period. The BESSs operate in accordance with the coordinated and coupled energy management system developed in this study.

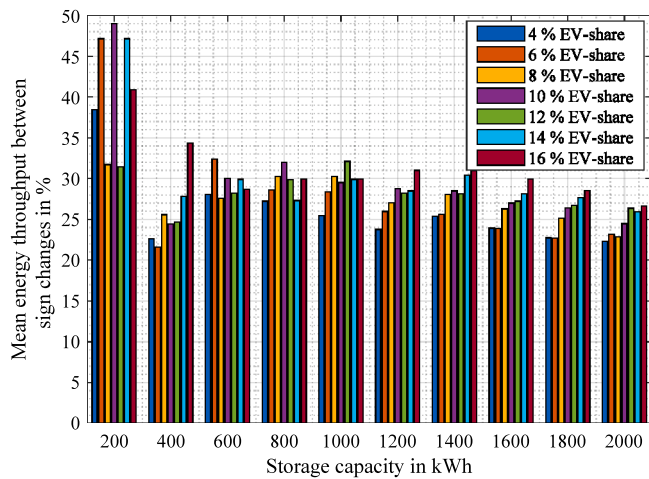


Fig. B.19. Average energy throughput between sign changes of the three battery energy storage systems (BESSs) after a six month simulation period. The BESSs operate in accordance with the coordinated and coupled energy management system developed in this study.

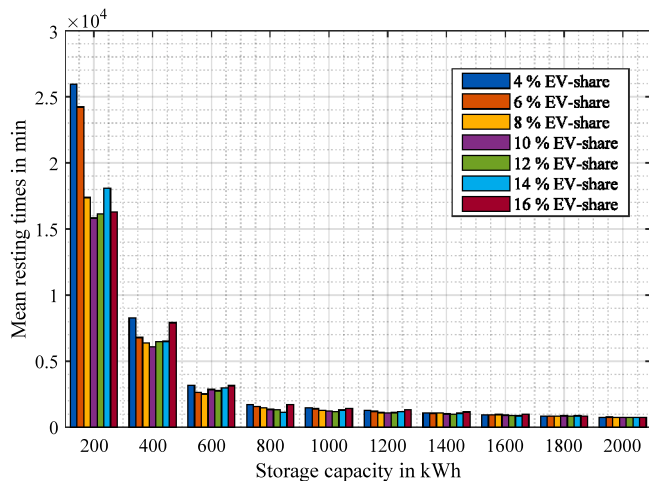


Fig. B.20. Average resting times of the three battery energy storage systems (BESSs) after a six month simulation period. The BESSs operate in accordance with the coordinated and coupled energy management system developed in this study.

References

[1] Richardson DB. Electric vehicles and the electric grid: A review of modeling approaches, impacts, and renewable energy integration. *Renew Sustain Energy Rev* 2013;19:247–54. <http://dx.doi.org/10.1016/j.rser.2012.11.042>.

[2] Crabtree G. The coming electric vehicle transformation. *Science* 2019;366(6464):422–4. <http://dx.doi.org/10.1126/science.aax0704>.

[3] Resch M, Bühler J, Klausen M, Sumper A. Impact of operation strategies of large scale battery systems on distribution grid planning in Germany. *Renew Sustain Energy Rev* 2017;74:1042–63. <http://dx.doi.org/10.1016/j.rser.2017.02.075>.

[4] Todts W, Mathieu L, Poliscanova J, Ambel CC, Muzi N, Alexandridou S. Recharge EU: How many charge points will Europe and its Member States need in the 2020s. URL <https://www.transportenvironment.org/sites/te/files/publications/01%202020%20Draft%20TE%20Infrastructure%20Report%20Final.pdf>.

[5] Nicholas M, Wappelhorst S. Regional charging infrastructure requirements in Germany through 2030. URL <https://theicct.org/sites/default/files/publications/germany-charging-infrastructure-20201021.pdf>.

[6] Galus MD, Vayá MG, Krause T, Andersson G. The role of electric vehicles in smart grids. *Wiley Interdiscip Rev: Energy Environ* 2013;2(4):384–400. <http://dx.doi.org/10.1002/wene.56>.

[7] Arias MB, Kim M, Bae S. Prediction of electric vehicle charging-power demand in realistic urban traffic networks. *Appl Energy* 2017;195:738–53. <http://dx.doi.org/10.1016/j.apenergy.2017.02.021>.

[8] Brinkel N, Schram WL, Alskaf TA, Lampropoulos I, van Sark W. Should we reinforce the grid? Cost and emission optimization of electric vehicle charging

under different transformer limits. *Appl Energy* 2020;276:115285. <http://dx.doi.org/10.1016/j.apenergy.2020.115285>.

[9] Pudjianto D, Djapic P, Aunedi M, Gan CK, Strbac G, Huang S, Infield D. Smart control for minimizing distribution network reinforcement cost due to electrification. *Energy Policy* 2013;52:76–84. <http://dx.doi.org/10.1016/j.enpol.2012.05.021>.

[10] Tan KM, Ramachandramurthy VK, Yong JY. Integration of electric vehicles in smart grid: A review on vehicle to grid technologies and optimization techniques. *Renew Sustain Energy Rev* 2016;53(Supplement C):720–32. <http://dx.doi.org/10.1016/j.rser.2015.09.012>.

[11] Kempton W, Tomić J. Vehicle-to-grid power implementation: From stabilizing the grid to supporting large-scale renewable energy. *J Power Sources* 2005;144(1):280–94. <http://dx.doi.org/10.1016/j.jpowsour.2004.12.022>.

[12] Sovacool BK, Noel L, Axsen J, Kempton W. The neglected social dimensions to a vehicle-to-grid (V2G) transition: a critical and systematic review. *Environ Res Lett* 2017;13(1):013001. <http://dx.doi.org/10.1088/1748-9326/aa9c6d>.

[13] Wang D, Coignard J, Zeng T, Zhang C, Saxena S. Quantifying electric vehicle battery degradation from driving vs. vehicle-to-grid services. *J Power Sources* 2016;332:193–203. <http://dx.doi.org/10.1016/j.jpowsour.2016.09.116>.

[14] Jafari M, Gauchia A, Zhao S, Zhang K, Gauchia L. Electric vehicle battery cycle aging evaluation in real-world daily driving and vehicle-to-grid services. *IEEE Trans Transp Electr* 2018;4(1):122–34. <http://dx.doi.org/10.1109/TTE.2017.2764320>.

[15] Hanemann P, Behnert M, Bruckner T. Effects of electric vehicle charging strategies on the German power system. *Appl Energy* 2017;203:608–22. <http://dx.doi.org/10.1016/j.apenergy.2017.06.039>.

[16] Hanemann P, Bruckner T. Effects of electric vehicles on the spot market price. *Energy* 2018;162:255–66. <http://dx.doi.org/10.1016/j.energy.2018.07.180>.

[17] Mehta R, Srinivasan D, Khambadkone AM, Yang J, Trivedi A. Smart charging strategies for optimal integration of plug-in electric vehicles within existing distribution system infrastructure. *IEEE Trans Smart Grid* 2018;9(1):299–312. <http://dx.doi.org/10.1109/TSG.2016.2550559>.

[18] Mehta R, Verma P, Srinivasan D, Yang J. Double-layered intelligent energy management for optimal integration of plug-in electric vehicles into distribution systems. *Appl Energy* 2019;233–234:146–55. <http://dx.doi.org/10.1016/j.apenergy.2018.10.008>.

[19] Diouf B, Pote R. Potential of lithium-ion batteries in renewable energy. *Renew Energy* 2015;76:375–80. <http://dx.doi.org/10.1016/j.renene.2014.11.058>.

[20] Hesse H, Martins R, Musilek P, Naumann M, Truong C, Jossen A. Economic optimization of component sizing for residential battery storage systems. *Energies* 2017;10(7):835. <http://dx.doi.org/10.3390/en10070835>.

[21] Gimelli A, Mottola F, Muccillo M, Proto D, Amoresano A, Andreotti A, Langella G. Optimal configuration of modular cogeneration plants integrated by a battery energy storage system providing peak shaving service. *Appl Energy* 2019;242:974–93. <http://dx.doi.org/10.1016/j.apenergy.2019.03.084>.

[22] Martins R, Hesse H, Jungbauer J, Vorbuchner T, Musilek P. Optimal component sizing for peak shaving in battery energy storage system for industrial applications. *Energies* 2018;11(8):2048. <http://dx.doi.org/10.3390/en11082048>.

[23] Reihani E, Motalleb M, Ghorbani R, Saad Saoud L. Load peak shaving and power smoothing of a distribution grid with high renewable energy penetration. *Renew Energy* 2016;86:1372–9. <http://dx.doi.org/10.1016/j.renene.2015.09.050>.

[24] Schram WL, Lampropoulos I, van Sark WG. Photovoltaic systems coupled with batteries that are optimally sized for household self-consumption: Assessment of peak shaving potential. *Appl Energy* 2018;223:69–81. <http://dx.doi.org/10.1016/j.apenergy.2018.04.023>.

[25] Nykamp S, Molderink A, Hurink JL, Smit GJM. Storage operation for peak shaving of distributed PV and wind generation. In: 2013 IEEE PES innovative smart grid technologies conference (ISGT). IEEE; 2013, p. 1–6. <http://dx.doi.org/10.1109/ISGT.2013.6497786>.

[26] Chapaloglou S, Nesiadis A, Iliadis P, Atsonios K, Nikolopoulos N, Grammelis P, Yiakopoulos C, Antoniadis I, Kakaras E. Smart energy management algorithm for load smoothing and peak shaving based on load forecasting of an island’s power system. *Appl Energy* 2019;238:627–42. <http://dx.doi.org/10.1016/j.apenergy.2019.01.102>.

[27] Purvins A, Sumner M. Optimal management of stationary lithium-ion battery system in electricity distribution grids. *J Power Sources* 2013;242:742–55. <http://dx.doi.org/10.1016/j.jpowsour.2013.05.097>.

[28] Englberger S, Hesse H, Kucevic D, Jossen A. A techno-economic analysis of vehicle-to-building: Battery degradation and efficiency analysis in the context of coordinated electric vehicle charging. *Energies* 2019;12(5):955. <http://dx.doi.org/10.3390/en12050955>.

[29] Naumann M, Truong CN, Schimpe M, Kucevic D, Jossen A, Hesse HC. SimSES: Software for techno-economic simulation of stationary energy storage systems. In: International ETG congress 2017. ETG-Fachbericht, Berlin and Offenbach: VDE Verlag; 2017, p. 442–7.

[30] Müller UP, Schachler B, Scharf M, Bunke W-D, Günther S, Bartels J, Pleßmann G. Integrated techno-economic power system planning of transmission and distribution grids. *Energies* 2019;12(11):2091. <http://dx.doi.org/10.3390/en12112091>.

- [31] Oudalov A, Cherkaoui R, Beguin A. Sizing and optimal operation of battery energy storage system for peak shaving application: 2007 IEEE lausanne power tech. In: IEEE PowerTech, 2007 IEEE Lausanne. 2007, p. 1–5. <http://dx.doi.org/10.1109/PCT.2007.4538388>.
- [32] German Federal Office of Justice. Stromnetzentgeltverordnung (in German): StromNEV. 2005, URL <https://www.gesetze-im-internet.de/stromnev/BJNR222500005.html>.
- [33] Englberger S, Hesse HC, Truong CN, Jossen A. Autonomous versus coordinated control of residential energy storage systems - monitoring profit, battery aging, and system efficiency. In: Schulz D, editor. NEIS 2018. Berlin: VDE VERLAG GMBH; 2019, p. 1–7, URL <http://ieeexplore.ieee.org/stamp/stamp.jsp?tp=&arnumber=8669465&isnumber=8669446>.
- [34] Kucevic D, Truong CN, Jossen A, Hesse HC. Lithium-ion battery storage design for buffering fast charging stations for battery electric vehicles and electric buses. In: Schulz D, editor. NEIS 2018. Berlin: VDE VERLAG GMBH; 2019, p. 1–6, URL <http://ieeexplore.ieee.org/stamp/stamp.jsp?tp=&arnumber=8669466&isnumber=8669446>.
- [35] Luo L, Gu W, Zhou S, Huang H, Gao S, Han J, Wu Z, Dou X. Optimal planning of electric vehicle charging stations comprising multi-types of charging facilities. Appl Energy 2018;226:1087–99. <http://dx.doi.org/10.1016/j.apenergy.2018.06.014>.
- [36] ABB. High power charging: Fast charging just got faster. High power for next generation electric vehicles.. 2020, URL <https://new.abb.com/ev-charging/products/car-charging/high-power-charging>.
- [37] Tjaden T, Bergner J, Weniger J, Quaschnig V. Repräsentative elektrische Lastprofile für Wohngebäude in Deutschland auf 1-sekündiger Datenbasis (in German). URL <https://pvspeicher.htw-berlin.de/daten/>.
- [38] Kucevic D, Tepe B, Englberger S, Parlikar A, Mühlbauer M, Bohlen O, Jossen A, Hesse H. Standard battery energy storage system profiles: Analysis of various applications for stationary energy storage systems using a holistic simulation framework. J Energy Storage 2020;28:101077. <http://dx.doi.org/10.1016/j.est.2019.101077>.
- [39] Kucevic D, Tepe B, Englberger S, Parlikar A, Muehlbauer M, Bohlen O, Jossen A, Hesse H. Standard battery energy storage system profiles: Dataset. URL <https://dataserv.ub.tum.de/s/m1510254/>.
- [40] Nobis C. Mobilität in Deutschland – MiD: Ergebnisbericht. URL <https://elib.dlr.de/125879/>.
- [41] Stadtwerke Kiel AG. Richtlinie zum netzanschluss für neu- und bestandsanschlüsse: Netzebene 5 – mittelspannung (MS). 2016, URL https://www.swkiel-netz.de/swkn/media/dokumente/netzanschluss/netzanschluss_strom/tabs/archiv/2016-03-03_RL_SWK_Netzanschluss.pdf.
- [42] Murata. Data sheet of sony fortelion US26650FTC1 battery cell. 2017, URL www.murata.com.
- [43] Naumann M, Schimpe M, Keil P, Hesse HC, Jossen A. Analysis and modeling of calendar aging of a commercial LiFePO₄/graphite cell. J Energy Storage 2018;17:153–69. <http://dx.doi.org/10.1016/j.est.2018.01.019>.
- [44] Naumann M, Spingler FB, Jossen A. Analysis and modeling of cycle aging of a commercial LiFePO₄/graphite cell. J Power Sources 2020;451:227666. <http://dx.doi.org/10.1016/j.jpowsour.2019.227666>.
- [45] Notton G, Lazarov V, Stoyanov L. Optimal sizing of a grid-connected PV system for various PV module technologies and inclinations, inverter efficiency characteristics and locations. Renew Energy 2010;35(2):541–54. <http://dx.doi.org/10.1016/j.renene.2009.07.013>.
- [46] Englberger S, Jossen A, Hesse H. Unlocking the potential of battery storage with the dynamic stacking of multiple applications. Cell Rep Phys Sci 2020;1. <http://dx.doi.org/10.1016/j.xcrp.2020.100238>.
- [47] Baumann M, Peters JF, Weil M, Grunwald A. CO₂ footprint and life-cycle costs of electrochemical energy storage for stationary grid applications. Energy Technol 2017;5(7):1071–83. <http://dx.doi.org/10.1002/ente.201600622>.
- [48] Naumann M, Karl RC, Truong CN, Jossen A, Hesse HC. Lithium-ion battery cost analysis in PV-household application. In: 9th International renewable energy storage conference, IRES 2015 73 (Supplement C). 2015, p. 37–47. <http://dx.doi.org/10.1016/j.egypro.2015.07.555>.
- [49] Truong CN, Naumann M, Karl RC, Müller M, Jossen A, Hesse HC. Economics of residential photovoltaic battery systems in Germany: The case of teslas powerwall. Batteries 2016;2(2):14. <http://dx.doi.org/10.3390/batteries2020014>.
- [50] Brown T, Hörsch J, Schlachtberger D. PyPSA: Python for power system analysis. J Open Res Softw 2018;6. <http://dx.doi.org/10.5334/jors.188>.
- [51] Müller UP, Schachler B, Bunke W-D, Bartels J, Glauer M, Büttner C, Günther Stephan, Kötter Editha, Cusmann I, Hülk L, Scharf M, Mossakowski T, Wendiggensen J. Netzebenenübergreifendes Planungsinstrument zur Bestimmung des optimalen Netz- und Speicherausbaus in Deutschland integriert in einer OpenEnergyPlattform: open_ego - Projektabschlussbericht. URL <https://www.uni-flensburg.de/fileadmin/content/abteilungen/industrial/dokumente/downloads/veroeffentlichungen/forschungsergebnisse/20190426endbericht-openeego-fkz0325881-final.pdf>.
- [52] Gurobi Optimization LLC. Gurobi optimization. 2020, URL <http://www.gurobi.com/>.